

Advanced Modeling and Simulation of Nanowire Field-Effect Sensors

S. Baumgartner,* M. Vasicek,** C. Heitzinger***

* *Wolfgang Pauli Institute c/o Department of Mathematics,
University of Vienna, A-1090 Vienna, Austria
(e-mail: Stefan.Baumgartner@univie.ac.at).*

** *Wolfgang Pauli Institute c/o Department of Mathematics,
University of Vienna, A-1090 Vienna, Austria
(e-mail: Martin.Vasicek@univie.ac.at)*

*** *Department of Applied Mathematics and Theoretical Physics
(DAMTP), University of Cambridge, Cambridge CB3 0WA, UK
(e-mail: C.Heitzinger@damtp.cam.ac.uk)*

Abstract: A 3d simulator for nanowire field-effect sensors and transistors including fast varying charge concentrations at an interface is presented. This simulator is based on a system of partial differential equations calculating the electrostatic potential of the whole device and the charge concentrations in the semiconducting nanowire. Therefore, three domains need to be modeled. The nanowire is described by the drift-diffusion-Poisson system, the Poisson-Boltzmann equation is used for the simulation of an aqueous solution, and the Poisson equation holds in the remaining oxide. Such devices can be used as gas sensors, and by functionalization of the nanowire surface, i.e., by attaching probe molecules, they can also be used for the detection of biomolecules in aqueous solutions. Binding of target molecules to the surface induces a field effect due to changes of charges in a small layer around the surface. This effect is responsible for the sensor response and hence is of paramount importance. A homogenization method resulting in two jump conditions is implemented which splits the computation into the charge of the boundary layer and into the remaining device. In order to take into account the geometry of the devices, 3d simulations are necessary and hence a parallelization technique has been developed. To include the jump conditions of the homogenization method, a novel finite-element tearing and interconnecting (FETI) method has been developed. With this simulator it is possible to solve the three dimensional and heterogeneous system of partial differential equations with discontinuities in feasible time using realizable computer power. As a result, sensitivity in terms of geometrical and physical properties can be predicted and sensors can be improved.

Keywords: NWFET, FETI, parallelization, PDE, drift-diffusion-Poisson system, Poisson-Boltzmann equation, homogenization, self-consistent, 3d simulations, nanowire sensor.

1. INTRODUCTION

Nanowire field-effect transistors (NWFETs) are attractive sensing devices with a wide range of applications; see Schöning and Poghossian (2006); Köck et al. (2009); Tian et al. (2010); Stern et al. (2010). For the detection of biomolecules, a nanowire of semiconducting material is covered with a dielectric layer functionalized with immobilized probe molecules (see Figure 1). In an electrolyte with target molecules, e.g., blood, the targets bind to the probes and in turn change the charge in a boundary layer, which induces a field effect. The same is valid for NWFET used for gas detection. Here the gas reacts with the nanowire surface and in turn changes the conductivity.

The advantage of nanowires for the purpose of detection is the small surface-to-volume ratio which gives high sensitivity and selectivity. Despite the experimental progress, many processes are not fully understood and hence modeling and simulation are crucial on the path to optimal sensing devices as described in Baumgartner et al. (2011).

The model and the techniques presented in this work can be used for both, for nanowire gas sensors and for nanowire biosensors; the techniques can also be used for field-effect transistors in general.

To characterize such devices, two important issues need to be solved, which result in high computational cost: the charges of the molecules are in Ångström range and the nanowire is of micrometer length, leading to a multiscale problem. Furthermore, a simplification to smaller dimensions than 3d is not possible due to the real-world boundary conditions breaking symmetry. Fortunately, we can reduce the computational cost without neglecting one of the two main parts, i.e., the transport in the nanowire and the reactions near the surface, by using a homogenization method, see Heitzinger et al. (2010). Then the charges at the different length scales can be computed separately in a self-consistent loop which allows to use the most suitable methods for the computation of both, the charges in the

boundary layer and the electrostatic potential of the whole device.

Models for charges of molecules in boundary layers in aqueous solutions can be of microscopic, macroscopic, or empirical character. Recently we have also used Metropolis Monte-Carlo simulations for the boundary layer charge of a DNA sensor, see Baumgartner et al. (2011). The remaining aqueous solution is modeled by the Poisson-Boltzmann equation and the transport in the nanowire is described by the drift-diffusion-Poisson system. Finally we get a system of PDES for which we proved existence and local uniqueness around thermal equilibrium and which can be solved self-consistently with an enhanced Scharfetter-Gummel iteration scheme, for details see Baumgartner and Heitzinger (2012). Nonetheless, the charge-transport problem is still a large linear system. Thus a parallelization technique is inevitable. In the following we describe the model equations and the parallelization technique in detail.

2. MODEL

The main goal of the simulations is to investigate the sensitivity of the functionalized NWFET device. Therefore we study the conductivity or current change due to the field effect. Hence we have to calculate the electrostatic potential in the whole device and the charge carriers, i.e., the electrons and the holes, in the nanowire. The simulation domain Ω consists of three material dependent parts: the nanowire Ω_{Si} , the dielectric layer Ω_{ox} , and the aqueous solution Ω_{liq} as depicted in Figure 1. The interface Γ is situated at the surface of the sensor and is defined as $\Gamma := \Omega_{ox} \cap \Omega_{liq}$.

The basic equation for the electrostatic potential is the Poisson equation

$$-\nabla \cdot (\varepsilon(\mathbf{x}) \nabla V(\mathbf{x})) = \rho(\mathbf{x}) \quad \text{in } \Omega, \quad (1a)$$

$$V(0+, x_2, x_3) = V(0-, x_2, x_3) \quad \text{on } \Gamma, \quad (1b)$$

$$\varepsilon_{liq} \partial_{x_1} V(0+, x_2, x_3) = \varepsilon_{ox} \partial_{x_1} V(0-, x_2, x_3) \quad \text{on } \Gamma, \quad (1c)$$

where V is the electrostatic potential, ρ is the charge concentration, and ε is the permittivity. The continuity conditions (1b) and (1c) are due to the different values of the permittivity ε between two materials. Here, for the sake of simplicity, the coordinate axes are chosen so that the interface is located at $x_1 = 0$. The same continuity equations hold at the interface between the silicon nanowire and the surrounding oxide due to the jump in the permittivity and will not be modified by the homogenization method since there is boundary layer to be homogenized.

Before we model the charge concentration in the boundary layer, we describe the charge concentration ρ in the remaining materials. In the semiconductor Ω_{Si} the Poisson equation is

$$-\nabla \cdot (\varepsilon_{Si} \nabla V) = q(p - n + C_{dop}) \quad (2)$$

and charge transport is described by the drift-diffusion equations

$$\nabla \cdot J_n = R, \quad (3a)$$

$$\nabla \cdot J_p = -R, \quad (3b)$$

$$J_n = D_n \nabla n - \mu_n n \nabla V, \quad (3c)$$

$$J_p = -D_p \nabla p - \mu_p p \nabla V, \quad (3d)$$

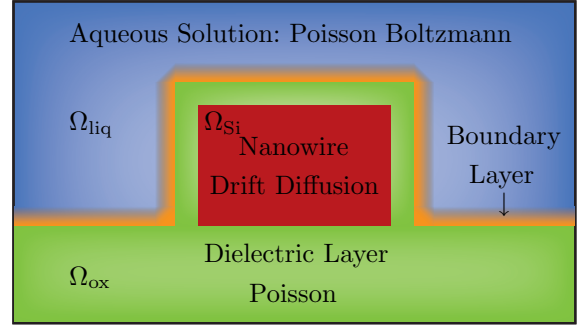


Fig. 1. Schematic cross section of the nanowire sensor; the different equations used in the simulation are indicated. The boundary layer includes probe molecules as well as target molecules bound to the probes.

where q is the elementary charge, C_{dop} is the doping concentration, n is the electron concentration, p is the hole concentration, D_n and D_p are the electron and hole diffusion coefficients, μ_n and μ_p are the corresponding mobilities, J_n and J_p are their current densities, and R denotes the recombination rate, see Markowich et al. (1990). In this work we use the Shockley-Read-Hall recombination rate

$$R := \frac{np - n_i^2}{\tau_p(n + n_i) + \tau_n(p + n_i)}, \quad (4)$$

where n_i denotes the intrinsic charge density and τ_n and τ_p are the relaxation times of the electrons and holes, respectively. Furthermore, we assume that the Einstein relations $D_n = U_T \mu_n$ and $D_p = U_T \mu_p$ hold, where U_T is the thermal voltage.

The screening of charges in the aqueous solution Ω_{liq} outside the boundary layer is described by the Poisson-Boltzmann equation

$$-\nabla \cdot (\varepsilon_{liq} \nabla V) = \sum_{\sigma \in \{-1, 1\}} \eta_\sigma e^{-\sigma \kappa V}, \quad (5)$$

where η is the ionic bulk concentration and the constant κ is defined as $\kappa := q/(kT)$, where k is the Boltzmann constant and T is the temperature. The right-hand side of equation (5) is the sum over all valences σ of ion species; for example, the set $\{-1, 1\}$ corresponds to a 1:1 electrolyte such as $\text{Na}^+ \text{Cl}^-$.

At the source, drain, and back-gate contacts, Dirichlet boundary conditions

$$V|_{\partial\Omega_S} = V_S, \quad n|_{\partial\Omega_S} = n_S, \quad p|_{\partial\Omega_S} = p_S, \quad (6a)$$

$$V|_{\partial\Omega_D} = V_D, \quad n|_{\partial\Omega_D} = n_D, \quad p|_{\partial\Omega_D} = p_D, \quad (6b)$$

$$V|_{\partial\Omega_G} = V_G \quad (6c)$$

hold. Sometimes an additional electrode is placed in the aqueous solution. This can also be modeled by a Dirichlet condition. Zero Neumann boundary conditions are used everywhere else.

As aforementioned, the charge concentration ρ is fast varying in the boundary layer and hence a homogenization method is suitable. After homogenization as in Heitzinger et al. (2010), the Poisson equation becomes

$$-\nabla \cdot (\varepsilon(\mathbf{x}) \nabla V(\mathbf{x})) = \begin{cases} \rho(\mathbf{x}) & \text{in } \Omega_{\text{Si}} \cup \Omega_{\text{ox}}, \\ 0 & \text{in } \Omega_{\text{liq}}, \end{cases} \quad (7a)$$

$$V(0+, \mathbf{y}) - V(0-, \mathbf{y}) = \alpha(\mathbf{y}) \quad \text{on } \Gamma, \quad (7b)$$

$$\varepsilon_{\text{liq}} \partial_{x_1} V(0+, \mathbf{y}) - \varepsilon_{\text{ox}} \partial_{x_1} V(0-, \mathbf{y}) = \beta(\mathbf{y}) \quad \text{on } \Gamma, \quad (7c)$$

where $0+$ denotes the limit at the interface on the side of the liquid, while $0-$ is the limit on the side of the oxide layer. The fast varying charge concentration in the surface layer is now subsumed in the macroscopic dipole-moment density α and the macroscopic surface-charge density β . Now we have to incorporate these conditions in the Scharfetter-Gummel iteration scheme, which is the standard method for the drift-diffusion-Poisson system.

3. SELF-CONSISTENT LOOP

The Scharfetter-Gummel iteration scheme consists of three steps: the calculation of the electrostatic potential V , of the electron density n , and of the hole density p . Our algorithm enhances this scheme by adding the calculation of the boundary layer charge which is dependent on the surface potential.

The first iteration with initial values n_0, p_0, α_0 , and β_0 works as follows:

- (1) Solve the boundary-value problem with interface conditions

$$-\nabla \cdot (\varepsilon \nabla V_1) = \begin{cases} q(p_0 - n_0 + C_{\text{dop}}) & \text{in } \Omega_{\text{Si}}, \\ 0 & \text{in } \Omega_{\text{ox}}, \\ -2\eta \sinh(\kappa V_1) & \text{in } \Omega_{\text{liq}}, \end{cases}$$

$$V_1(0+, \mathbf{y}) - V_1(0-, \mathbf{y}) = \alpha_0(\mathbf{y}) \quad \text{on } \Gamma,$$

$$\varepsilon(0+) \partial_{x_1} V_1(0+, \mathbf{y})$$

$$- \varepsilon(0-) \partial_{x_1} V_1(0-, \mathbf{y}) = \beta_0(\mathbf{y}) \quad \text{on } \Gamma,$$

$$V_1 = V_D \quad \text{on } \partial\Omega_D,$$

$$\nabla_\nu V_1 = 0 \quad \text{on } \partial\Omega_N$$

for V_1 .

- (2) Solve the elliptic boundary-value problem

$$\nabla \cdot (D_n \nabla n_1 - \mu_n n_1 \nabla V)$$

$$= \frac{n_1 p_0 - n_i^2}{\tau_p(n_1 + n_i) + \tau_n(p_0 + n_i)} \quad \text{in } \Omega_{\text{Si}},$$

$$n_1 = n_D \quad \text{on } \partial\Omega_D,$$

$$\nabla_\nu n_1 = 0 \quad \text{on } \partial\Omega_N$$

for n_1 . Here the n_1 in the denominator can be replaced by n_0 which makes the discretized system linear.

- (3) Solve the elliptic boundary-value problem

$$\nabla \cdot (D_p \nabla p_1 + \mu_p p_1 \nabla V)$$

$$= \frac{n_1 p_0 - n_i^2}{\tau_p(n_1 + n_i) + \tau_n(p_1 + n_i)} \quad \text{in } \Omega_{\text{Si}},$$

$$p_1 = p_D \quad \text{on } \partial\Omega_D,$$

$$\nabla_\nu p_1 = 0 \quad \text{on } \partial\Omega_N$$

for p_1 .

- (4) Update the surface-charge density and dipole-moment density according to a boundary model

$$\alpha_1(y) := M_\alpha(V_1),$$

$$\beta_1(y) := M_\beta(V_1),$$

where M_α and M_β are the functions giving the densities according to the surface potentials. In the

case of Monte-Carlo simulations, this can be done by generating a look-up table with density values for different surface voltages.

4. FETI METHOD

The 3d charge transport problem is still large and consequently we derived a novel finite element tearing and interconnecting (FETI) method based on the work of Farhat and Roux (1991) including the coupled system of the Poisson drift-diffusion system, the linearized Poisson-Boltzmann equation, and jump conditions arising from the homogenization method.

Therefore we discretize the boundary-value problems in the self-consistent loop by a finite-volume method. Instead of solving the whole domain Ω , we split the domain in N boxes as depicted for a simple example of 9 boxes in a cross section in Figure 2. The domain can be further divided in the remaining coordinate direction.

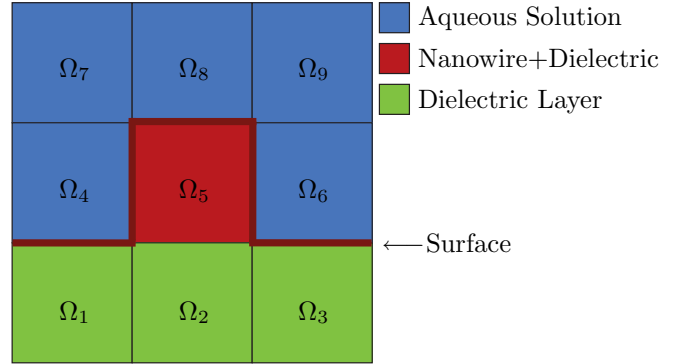


Fig. 2. Splitting of the domain in the x - y cross section. In order to implement the jumps at the surface, the border of the boxes coincide with the surface. Only in the nanowire box two different materials arise. Everywhere else only one material is present and hence the computation can be improved.

The discretized linear systems on each of the N boxes can be written as $A_i u_i = f_i$, $i \in (1, \dots, N)$ with

$$A_i = \begin{pmatrix} A_{II}^i & A_{I\Gamma}^i \\ A_{\Gamma I}^i & A_{\Gamma\Gamma}^i \end{pmatrix}. \quad (12)$$

It is convenient to transform this system into the Schur complement which reduces the whole problem to a problem on the boundary, i.e.,

$$S_i := A_{\Gamma\Gamma}^i - A_{\Gamma I}^i (A_{II}^i)^{-1} A_{I\Gamma}^i. \quad (13)$$

In the following we write instead of u_Γ^i from $u_i = (u_I^i, u_\Gamma^i)$ again u_i . A solution of the Schur complement system and hence also on the whole domain can be obtained by solving the minimization problem

$$J(u) := \frac{1}{2} \langle Su, u \rangle - \langle g, u \rangle = \min!, \quad (14a)$$

$$Bu = \alpha, \quad (14b)$$

where

$$u = \begin{pmatrix} u_1 \\ u_2 \\ \vdots \\ u_N \end{pmatrix}, \quad g = \begin{pmatrix} g_1 \\ g_2 \\ \vdots \\ g_N \end{pmatrix}, \quad S = \begin{pmatrix} S_1 & 0 & \cdots & 0 \\ 0 & S_2 & \ddots & \vdots \\ \vdots & \ddots & \ddots & 0 \\ 0 & \cdots & 0 & S_N \end{pmatrix}$$

and B is the connectivity matrix containing only elements of $\{-1, 0, 1\}$. The right-hand sides f_i are modified by the transformation to the Schur complement and by adding of β . The jump condition β arises in the discretized right-hand side due to the weak formulation of the boundary value problem. Hence in the following we need only to know where we have to implement α in our procedure.

But first we have to think about our Schur complements which could be singular for some reasons, e.g., when the boundary conditions are ill posed. Therefore we introduce the matrix R of null-space elements of S as

$$R := \begin{pmatrix} R_1 & 0 & \cdots & 0 \\ 0 & R_2 & \ddots & \vdots \\ \vdots & \ddots & \ddots & 0 \\ 0 & \cdots & 0 & R_N \end{pmatrix}. \quad (15)$$

Now we do two steps: we implement the matrix R and include the constraint $Bu = \alpha$ of our minimization problem by introducing Lagrange multipliers λ . By introducing some variables, the solution of the minimization problem (14) can be obtained by solving

$$F\lambda + G\gamma = d, \quad (16a)$$

$$G^T\lambda = e, \quad (16b)$$

where $F := BS^\dagger B^T$, $G := BR$, $d := BS^\dagger g - \alpha$, and $e := R^T g$. This system is now in the same form as the original FETI method. The aim is to solve this system with a preconditioned conjugate gradient method. Therefore we use the projection

$$P^T := I - G(G^T QG)^{-1} G^T Q \quad (17)$$

with a scaling matrix Q which reduces the system (16) to

$$P^T F \lambda = P^T d, \quad (18a)$$

$$G^T \lambda = e. \quad (18b)$$

In every step of (1)-(3) in the self-consistent loop we have to use the cg method. Hence it is of interest to keep the number of iterations in every cg computation small, which can be improved by using a preconditioner M , i.e., we have to solve the equations

$$PM^{-1}P^T F \lambda = PM^{-1}P^T d, \quad (19a)$$

$$G^T \lambda = e. \quad (19b)$$

For heterogeneous systems it is recommended to use the Dirichlet preconditioner

$$M^{-1} = B_D S B_D^T \quad (20)$$

or the lumped preconditioner

$$M^{-1} = B_D A_{\Gamma\Gamma} B_D^T \quad (21)$$

as defined in Klawonn and Rheinbach (2010) where B_D is the connectivity matrix B multiplied with scaling matrices including the permittivity ε or the multiplicity of the boxes involved in the degrees of freedom at the interface. A comparison of these preconditioners can be found in Rixen and Farhat (1999). The cg method looks as follows, see also Toselli and Widlund (2005), p. 149.

Initialize the first Lagrange multiplier and the first residuum

$$\lambda_0 = QG(G^T QG)^{-1} e + \mu, \quad \mu \in \text{range}(P) \\ r_0 = d - F\lambda_0$$

For $k = 1, 2, \dots$ until convergence

$$\text{Project : } q_{k-1} = P^T r_{k-1}$$

$$\text{Precondition : } z_{k-1} = M^{-1} q_{k-1}$$

$$\text{Project : } y_{k-1} = P z_{k-1}$$

$$\beta_1 = 0 \text{ and } \beta_k = \langle y_{k-1}, q_{k-1} \rangle / \langle y_{k-2}, q_{k-2} \rangle$$

$$p_1 = y_0 \text{ and } p_k = y_{k-1} + \beta_k p_{k-1}$$

$$\alpha_k = \langle y_{k-1}, q_{k-1} \rangle / \langle p_k, F p_k \rangle$$

$$\lambda_k = \lambda_{k-1} + \alpha_k p_k$$

$$r_k = r_{k-1} - \alpha_k F p_k$$

5. RESULTS

To show the correct implementation of the jump conditions we simulate a device with a cross section as shown in Figure 2. For the following example we keep the dimensions small and take boxes with the size $10 \times 10 \times 10$ and a total length, in z -direction, of 20. Hence the whole simulation domain consists of 18 blocks. Furthermore we apply 0.01 V backgate voltage, i.e., at $y = 0$, and 0.05 V at the source, i.e., in Ω_{S_i} at $z = 0$. All other constants in the drift-diffusion-Poisson system are chosen as in Markowich et al. (1990), where room temperature is assumed.

As aforementioned, the jump conditions are given by the boundary-layer model. For the sake of simplicity, this part of the model is not discussed and we use the jump conditions

$$V(0+, \mathbf{y}) - V(0-, \mathbf{y}) = -0.003, \quad (22a)$$

$$\varepsilon_{\text{liq}} \partial_{x_1} V(0+, \mathbf{y}) - \varepsilon_{\text{ox}} \partial_{x_1} V(0-, \mathbf{y}) = 0.00001. \quad (22b)$$

At the cross section $z = 10$ in Figure 3 we can see the backgate condition on the left, the electrostatic potential of the drift-diffusion-Poisson system in the middle and the aqueous solution (dark green). The jump conditions are clearly depicted between the oxide and the aqueous solution.

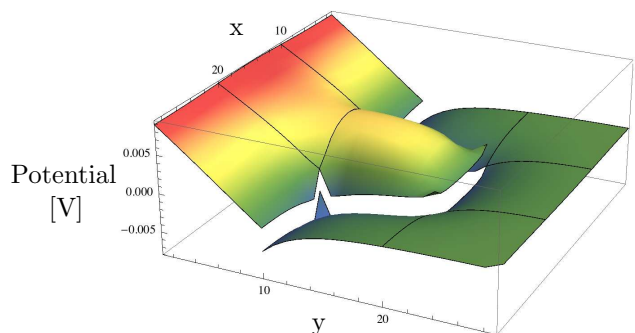


Fig. 3. Cross section of the electrostatic potential at $z = 10$.

The symmetric structure of the device can be seen at the cross section $y = 15$ in Figure 4. Here we have the solution of the Poisson drift-diffusion system and the Poisson equation with vanishing right-hand side in the

middle, and the aqueous solution on the left and right of it. Between $12 \leq x \leq 18$ at $z = 0$ the Dirichlet conditions for the source contact hold. Again the jump conditions can be clearly seen.

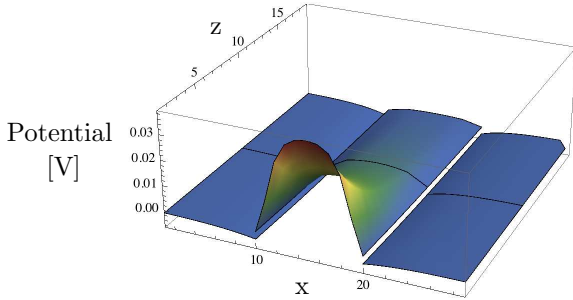


Fig. 4. Cross section of the electrostatic potential at $y = 15$.

The same Dirichlet conditions for the source contact are visible at the cross section $x = 15$ in Figure 5. Here we have at the left the oxide, in the middle the silicon covered by an oxide layer, and at the right the aqueous solution separated from the oxide by the jump conditions.

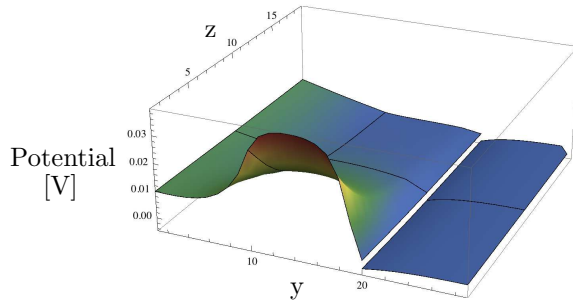


Fig. 5. Cross section of the electrostatic potential at $x = 15$.

As aforementioned the choice of the preconditioner is important for the reduction of computation time. Please note that in our simulations no projections are needed due to non-singular Schur complements on the subdomains. We tested the Dirichlet preconditioner (20) and the lumped preconditioner (21) without scaling, i.e., $B_D = B$, with multiplicity scaling, and with ε -scaling (see Table 1).

Therefore we simulate the same device as in Figure 3 with half dimensions in every coordinate direction. Hence we have $15 \times 15 \times 10 = 2250$ degrees of freedom and blocks with dimensions $5 \times 5 \times 5$.

Preconditioner	Scaling	Iterations
Dirichlet	without	207
Lumped		204
Dirichlet	multiplicity	389
Lumped		445
Dirichlet	ε	339
Lumped		463

Table 1. Iteration number for Dirichlet and lumped preconditioners without scaling, with multiplicity scaling and ε scaling.

In our simulations the preconditioners without scalings perform best. No significant difference between the non-

scaled Dirichlet and the non-scaled lumped preconditioner can be found. As in Rixen and Farhat (1999), the ε -scaled Dirichlet preconditioner perform better than the multiplicity scaled Dirichlet preconditioner and the simulations with scaled and lumped preconditioners need more iterations.

After a boundary-layer model is chosen, the different physical and geometrical properties of NWFET devices can be tested for their influence on the sensitivity of the sensor, see Baumgartner et al. (2011). The sensitivity can be expressed as the change of current or as change of conductivity. We modeled a DNA sensor with different nanowire thicknesses as an example, see Figure 6. Here the field effect results from the binding of ssDNA strands to corresponding strands functionalized at the surface. Hence we have to compute the current of the DNA sensor without functionalization, i.e., no molecules are present in the boundary layer, with ssDNA attached at the surface, and with dsDNA bound to the surface. The difference of the resulting currents, i.e., the sensitivity, is depicted in Figure 6.

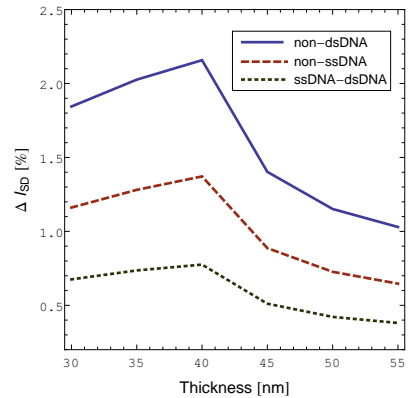


Fig. 6. Simulations of sensitivity as current change in terms of nanowire thickness due to different charges at the surface of a DNA sensor. The molecules in the boundary layer are dsDNA or ssDNA strands.

The resulting sensitivity in Figure 6 shows an optimal point for a NWFET device with a 40 nm thick nanowire. Hence an improvement of this sensor can be obtained by changing the nanowire thickness. For other improvements see Baumgartner et al. (2011)

6. CONCLUSION

The simulation of NWFET devices is difficult due to the inherent multiscale problem and the high computational cost of 3d simulations. In this work the multiscale problem is solved by a homogenization method resulting in jump conditions and the computation time can be reduced by a novel FETI algorithm. This method includes the drift-diffusion-Poisson system, a Poisson-Boltzmann model, and jump conditions.

It is now possible to study such nanowire bio- and gas sensors from a physical and geometrical point of view. Our investigations help to understand devices based on NWFETs quantitatively and give guidelines how to reach optimal sensitivity, see Baumgartner et al. (2011).

ACKNOWLEDGEMENTS

The authors acknowledge support by the FWF (Austrian Science Fund) project No. P20871-N13. This work has been funded by the Vienna Science and Technology Fund (WWTF) by project No. MA09-028. This publication is based on work supported by Award No. KUK-I1-007-43, funded by the King Abdullah University of Science and Technology (KAUST). Simulations are performed on the Vienna Scientific Cluster (vsc).

REFERENCES

- Baumgartner, S. and Heitzinger, C. (2012). Existence and local uniqueness for 3d self-consistent multiscale models of field-effect sensors. *Commun. Math. Sci.*, 10(2), 693–716.
- Baumgartner, S., Vasicek, M., Bulyha, A., and Heitzinger, C. (2011). Optimization of nanowire DNA sensor sensitivity using self-consistent simulation. *Nanotechnology*, 22(42), 425503/1–8.
- Farhat, C. and Roux, F. (1991). A method of finite element tearing and interconnecting and its parallel solution algorithm. *Int. J. Numer. Methods Eng.*, 32(6), 1205–1227.
- Heitzinger, C., Mauser, N., and Ringhofer, C. (2010). Multiscale modeling of planar and nanowire field-effect biosensors. *SIAM J. Appl. Math.*, 70(5), 1634–1654.
- Klawonn, A. and Rheinbach, O. (2010). Highly scalable parallel domain decomposition methods with an application to biomechanics. *ZAMM*, 90(1), 5–32.
- Köck, A., Tischner, A., Maier, T., Kast, M., Edtmaier, C., Gspan, C., and Kothleitner, G. (2009). Atmospheric pressure fabrication of SnO₂-nanowires for highly sensitive CO and CH₄ detection. *Sens. Actuators, B*, 138(1), 160–167.
- Markowich, P., Ringhofer, C., and Schmeiser, C. (1990). *Semiconductor Equations*. Springer-Verlag New York, Inc. New York, NY, USA.
- Rixen, D. and Farhat, C. (1999). A simple and efficient extension of a class of substructure based preconditioners to heterogeneous structural mechanics problems. *Int. J. Numer. Methods Eng.*, 44(4), 489–516.
- Schöning, M. and Poghossian, A. (2006). Bio FEDs (field-effect devices): State-of-the-art and new directions. *Electroanal.*, 18(19–20), 1893–1900.
- Stern, E., Vacic, A., Rajan, N., Criscione, J., Park, J., Ilic, B., Mooney, D., Reed, M., and Fahmy, T. (2010). Label-free biomarker detection from whole blood. *Nat. Nanotechnol.*, 5(2), 138–142.
- Tian, B., Cohen-Karni, T., Qing, Q., Duan, X., Xie, P., and Lieber, C. (2010). Three-dimensional, flexible nanoscale field-effect transistors as localized bioprobes. *Science*, 329(5993), 830–834.
- Toselli, A. and Widlund, O. (2005). *Domain Decomposition Methods—Algorithms and Theory*, volume 34 of *Springer Series in Computational Mathematics*. Springer Verlag.